

**Quantitative analysis of neuronal mitochondrial movement reveals patterns resulting from neurotoxicity of rotenone and 6-hydroxydopamine**

**Author**

Simões, Rui F, Pino, Rute, Moreira-Soares, Maurício, Kovarova, Jaromira, Neuzil, Jiri, Travasso, Rui, Oliveira, Paulo J, Cunha-Oliveira, Teresa, Pereira, Francisco B

**Published**

2021

**Journal Title**

FASEB Journal

**Version**

Accepted Manuscript (AM)

**DOI**

<https://doi.org/10.1096/fj.202100899R>

**Copyright Statement**

© 2021 Federation of American Societies for Experimental Biology. This is the author-manuscript version of this paper. Reproduced in accordance with the copyright policy of the publisher. Please refer to the journal website for access to the definitive, published version.

**Downloaded from**

<http://hdl.handle.net/10072/410518>

**Griffith Research Online**

<https://research-repository.griffith.edu.au>

1 **Quantitative analysis of neuronal mitochondrial movement reveals patterns**  
2 **resulting from neurotoxicity of rotenone and 6-hydroxydopamine**

3  
4 Authors: Rui F. Simões<sup>1</sup>, Rute Pino<sup>2</sup>, Maurício Moreira-Soares<sup>3,4</sup>, Jaromira Kovarova<sup>5</sup>,  
5 Jiri Neuzil<sup>5,6</sup>, Rui Travasso<sup>7</sup>, Paulo J. Oliveira<sup>1</sup>, Teresa Cunha-Oliveira<sup>1</sup>, Francisco B.  
6 Pereira<sup>2,8</sup>

7  
8 Affiliations:

9 1 - CNC, Center for Neuroscience and Cell Biology, UC Biotech, Biocant Park, 3060-197  
10 Cantanhede, Portugal

11 2 - CISUC, Department of Informatics Engineering, University of Coimbra, 3030 Coimbra,  
12 Portugal

13 3 - OCBE, Faculty of Medicine, University of Oslo, Oslo, Norway

14 4 - Centre for Bioinformatics, Faculty of Mathematics and Natural Sciences, University of Oslo,  
15 Oslo, Norway

16 5 - Institute of Biotechnology, Czech Academy of Sciences, 252 50 Prague-West, Czech  
17 Republic

18 6 - School of Medical Science, Griffith University, Southport, 4222 Qld, Australia

19 7 - CFisUC, Department of Physics, University of Coimbra, 3004-516 Coimbra, Portugal

20 8 - Coimbra Polytechnic - ISEC, 3030-190 Coimbra, Portugal

21  
22 Corresponding author:

23 #Teresa Cunha-Oliveira, MitoXT (Mitochondrial Toxicology and Experimental Therapeutics  
24 Laboratory), CNC, Center for Neuroscience and Cell Biology, UC Biotech Building (Lote 8A),  
25 Biocant Park, 3060-197 Cantanhede, Portugal; phone: +351 231249170 (ext 715); fax: +351  
26 231249179; email: teresa.oliveira@uc-biotech.pt; teresa.oliveira@gmail.com

28 **Keywords:** Live cell imaging; Mitochondria movement; Trajectory descriptors;  
29 Neurotoxicants; Exploratory data analysis; Principal component analysis.

30

31 **Abbreviations:** 6-OHDA, 6-hydroxydopamine; ATP, adenosine triphosphate; BSA,  
32 bovine serum albumin; Ca<sup>2+</sup>, calcium; fps, frames per second; MIRO, mitochondrial rho;  
33 PCA, Principal Component Analysis; PBS, phosphate buffer saline; RA, retinoic Acid;  
34 TIRF, Total internal reflection fluorescence; TRAK, trafficking kinesin-binding.

35

36 **Abstract**

37

38 Alterations in mitochondrial dynamics, including their trafficking, can present early  
39 manifestation of neuronal degeneration. However, current methodologies used to study  
40 mitochondrial trafficking events rely on parameters that are mostly altered in later stages  
41 of neurodegeneration. Our objective was to establish a reliable computational  
42 methodology to detect early alterations in neuronal mitochondrial trafficking. We propose  
43 a novel quantitative analysis of mitochondria trajectories based on innovative movement  
44 descriptors, including straightness, efficiency, anisotropy, and kurtosis. Using biological  
45 data from differentiated SH-SY5Y cells treated with mitochondrial toxicants 6-  
46 hydroxydopamine and rotenone, we evaluated time and dose-dependent alterations in  
47 trajectory descriptors. Mitochondrial movement was analyzed by total internal reflection  
48 fluorescence microscopy followed by computer modelling to describe the process. The  
49 stacks of individual images were analyzed by an open source MATLAB algorithm  
50 ([www.github.com/kandelj/MitoSPT](http://www.github.com/kandelj/MitoSPT)) and to characterize mitochondria trajectories, we  
51 used the Python package trajpy (<https://github.com/ocbe-uio/trajpy/>). Our results  
52 confirm that this computational approach is effective and accurate in order to study  
53 mitochondrial motility and trajectories in the context of healthy and diseased neurons in  
54 different stages.

55

56

57 **1. Introduction**

58

59 Neurons are polarized post-mitotic cells encompassing three structurally, functionally,  
60 and metabolically distinct domains, i.e. the cell body, dendrites with numerous branches,  
61 and the axon. These domains display unique metabolic and energetic needs, and they rely  
62 on mitochondrial adenosine triphosphate (ATP) production to accomplish their specific  
63 functions (1-3). Mitochondria-produced ATP is vital for neuronal cell growth and  
64 survival, synapse formation and assembly, generation of action potentials, synaptic  
65 transmission and synaptic vesicle trafficking (4-6). Additionally, mitochondria are also  
66 pivotal in calcium ( $\text{Ca}^{2+}$ ) homeostasis in neuronal cells, buffering transient  $\text{Ca}^{2+}$  levels by  
67 its sequestration and release, as needed (7, 8). As individual neuronal domains feature  
68 specific needs for the level of  $\text{Ca}^{2+}$  as well as metabolites, their homeostasis is maintained  
69 by corresponding number of mitochondria (1, 9, 10).

70 Due to their morphological and metabolic characteristics, neuronal cells have developed  
71 mechanisms to transport mitochondria along microtubular tracks. The movement from  
72 the cell body to cellular extremities (anterograde transport) is mediated by the kinesin-1  
73 family proteins, while dynein proteins are responsible for the opposite movement  
74 (retrograde transport). Both types of transport are dependent on ATP hydrolysis (11, 12).

75 Movement of mitochondria is dependent on the polarity of microtubules, polymeric  
76 structures composed of  $\alpha$ - and  $\beta$ - tubulin, that polymerize from the minus to the plus end.

77 In axons, the minus end is directed towards the cell body and the plus end to the cell  
78 extremity (13, 14). Thus, kinesins carry mitochondria from the minus to the plus end and  
79 dyneins from the plus to the minus end (15).

80 Mitochondrial trafficking is also dependent on adaptor proteins, which ensure targeted  
81 and efficient transport regulation. The trafficking kinesin-binding (TRAK) proteins 1 and  
82 2 bridge the mitochondrial rho (MIRO) 1 and 2 proteins and kinesins to control

83 mitochondrial anterograde trafficking (16, 17). Relevant for the retrograde transport,  
84 dynactin binds to dynein and to the microtubules, enhancing dynein motor processivity  
85 (11, 18). Mitochondrial docking processes allow mitochondria to remain stationary in  
86 areas with elevated ATP demand and  $\text{Ca}^{2+}$  buffering dependency (1). It has been described  
87 that between 10% and 40% of mitochondria in a neuronal cell are in motion, while 60%  
88 to 90% of the organelles are stationary (10, 19, 20).

89 Since mitochondria are physically allocated to areas with higher metabolic activity and  
90 also based on regulation of  $\text{Ca}^{2+}$  homeostasis, aberrations in mitochondrial dynamics,  
91 metabolism and mobility, leading to altered ATP production and lower  $\text{Ca}^{2+}$  buffering  
92 capacity, are involved in the development of neurodegenerative pathologies, such as  
93 Alzheimer's disease, Huntington's disease, Parkinson's disease, and amyotrophic lateral  
94 sclerosis (1). Furthermore, it was previously shown that alterations in mitochondrial  
95 motility appear prior to the first signs of neurodegeneration (such as degeneration of  
96 axons and cell death) (21, 22).

97 Mitochondria move along short or long paths with varying velocities and directions, often  
98 altering those parameters as a response to different stimuli (23). Additionally,  
99 mitochondria undergo morphological alterations during movement, posing an increased  
100 challenge in the identification and segmentation of individual mitochondria. A further  
101 obstacle is the low signal-to-noise ratio of many microscopic approaches, yielding poor  
102 quality images (24). Associated video acquisition processes can be detrimental due to  
103 photobleaching and phototoxicity (25). Therefore, the videos taken under these  
104 microscopy approaches are either short (2-5 min) with 1-2 frames per second (fps) (20,  
105 24, 26) or longer (30 min) but with 1 frame every 5-10 s (27). Short videos cannot collect  
106 all features required to characterize mitochondrial motion while in longer movies,  
107 important information may be lost between frames.

108 To circumvent the limitations described, we used here total internal reflection  
109 fluorescence (TIRF) microscopy that takes advantage of a special mode of sample  
110 illumination, exciting only fluorophores located near the sample interface (about 100 nm),  
111 without exciting sample regions located further away. Images obtained with this  
112 microscopy technique present higher signal-to-noise ratio and almost nonexistent out-of-  
113 focus fluorescence, preventing photobleaching and phototoxicity (28-30).

114 We exposed the cells to mitochondrial toxins, evaluated the mitochondrial movement by  
115 TIRF microscopy, and used computer modelling to describe the process. Our results  
116 present a new quantitative paradigm of mitochondrial dynamics in health and diseased  
117 neuronal cells.

118

## 119 **2. Results**

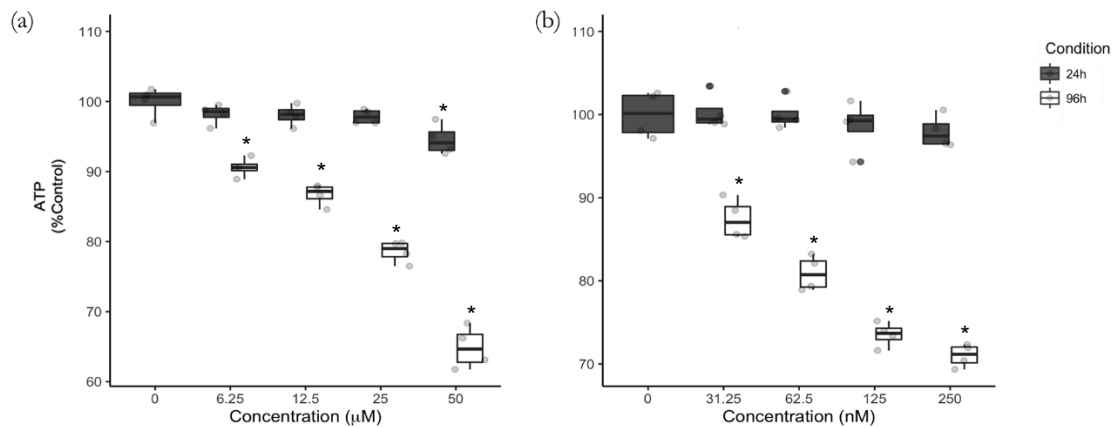
120

### 121 **2.1. 6-OHDA and rotenone decreased ATP levels in a concentration and time-** 122 **dependent manner.**

123

124 Mitochondrial trafficking in neuronal cells is highly dependent on ATP consumption,  
125 since kinesin and dynein transport requires ATP hydrolysis (Hirokawa et al. 2010). We  
126 initially measured cellular ATP levels after treating cells for 24 h and 96 h with 6-OHDA  
127 (Fig 1 a) and rotenone (Fig 1). While there was little if any effect of the agents at 24 h,  
128 96h-treatment caused considerable decrease in ATP levels (Fig 1).

129



130

131

132 **Fig 1 – Treatment with 6-OHDA (a) and rotenone (b) for 24h and 96 h causes different decreases of**  
 133 **ATP levels.**

134 Differentiated SH-SY5Y cells were treated with 6-OHDA (a) or rotenone (b) for 24 and 96 h. Data are  
 135 presented as boxplots, in which each dot represents an independent cell population (n=4), in duplicate.  
 136 Kruskal-Wallis test (one-way ANOVA on ranks) pairwise (control vs 6-OHDA or control vs rotenone) was  
 137 used to assess statistical significance, (\*) p < 0.05.

138

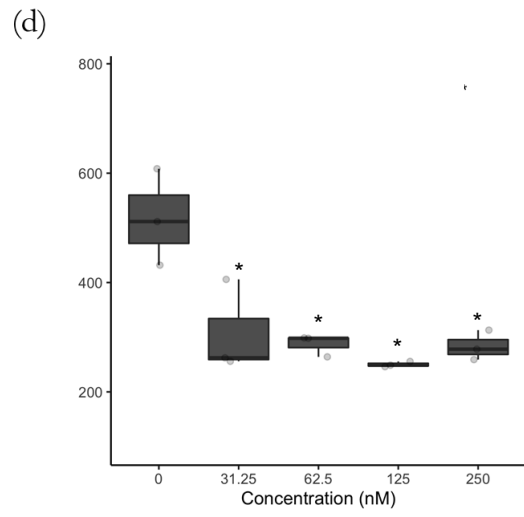
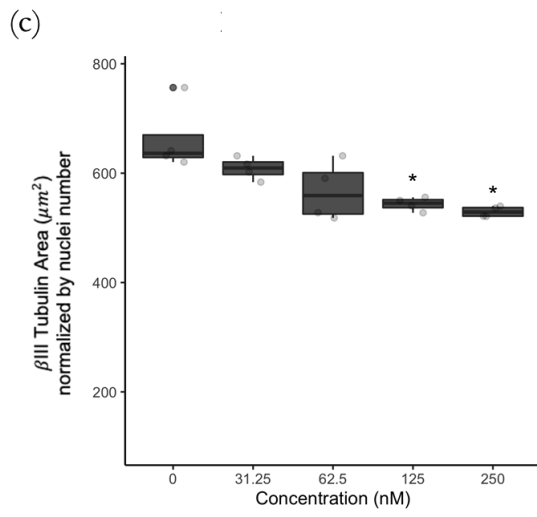
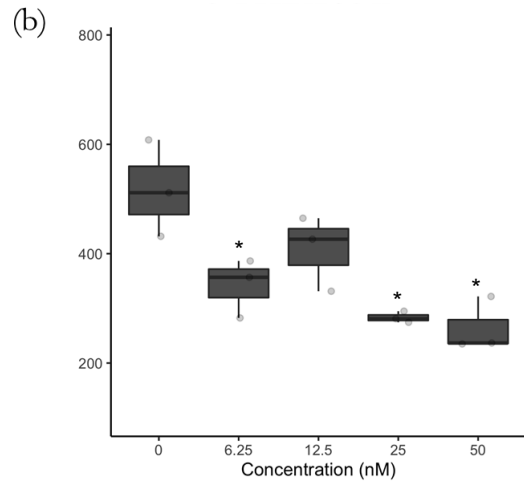
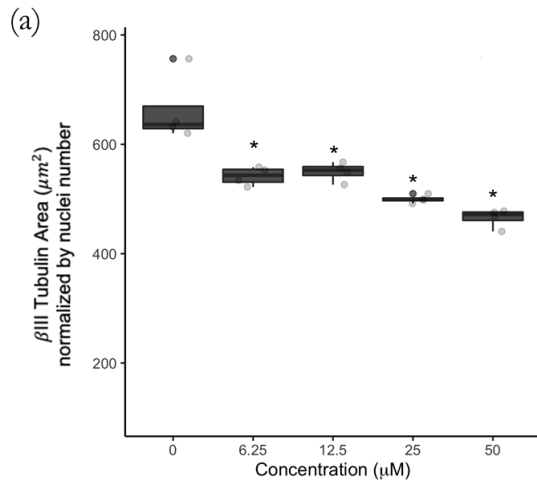
139 **2.2. 6-OHDA and rotenone reduced the level of βIII tubulin.**

140

141 We next tested the effect of 6-OHDA and rotenone on tubulin levels in differentiated SH-  
 142 SY5Y cells. All 6-OHDA treatments (except 12.5 μM for 96 h) significantly decreased  
 143 the levels of tubulin (Fig 2 a and b). Regarding rotenone, 125 nM and 250 nM for the 24-  
 144 h time point induced an evident decreased in tubulin levels (Fig 2 c). This effect was  
 145 considerably stronger for the 96-h treatment (Fig 2 d). Representative images (Fig 2 e and  
 146 f) of cells treated with different concentrations of 6-OHDA (ii-v) and rotenone (vi-ix) for  
 147 24 h (e) and 96 h (f) are presented below.

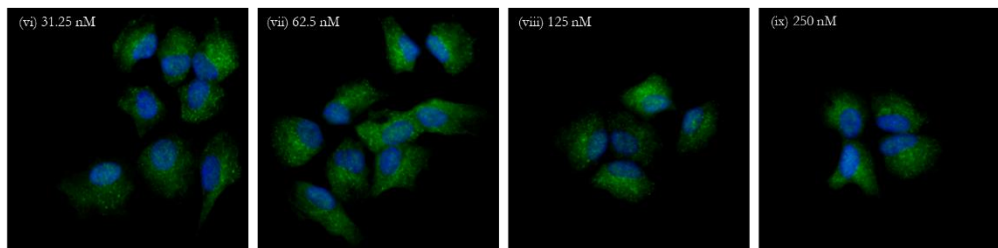
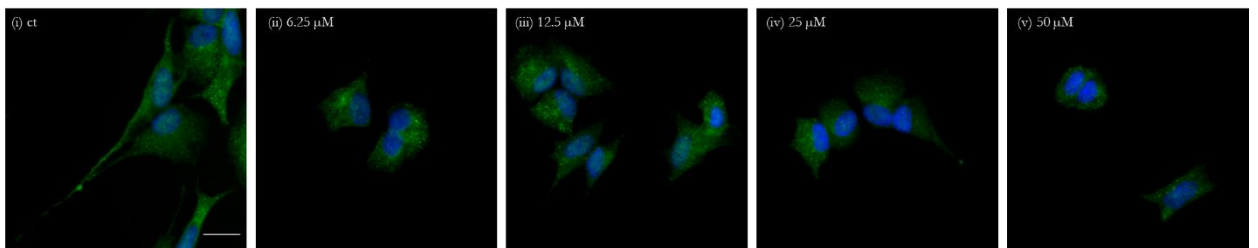
148





149

(e) 24 h 150



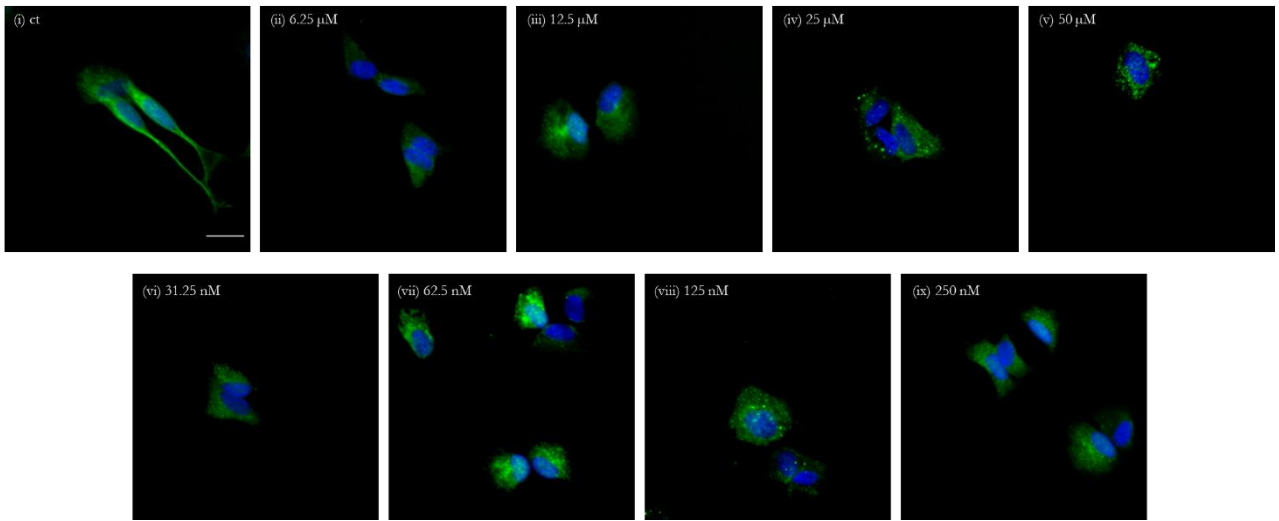
151

152

153

154

155

(f) 96 h <sup>157</sup>

158

159

160

161

162

163 **Fig 2 – Incubations with 6-OHDA and rotenone decreases the level of  $\beta$ III tubulin in a dose-**  
 164 **dependent manner.**

165 Incubations with 6-OHDA for 24 h (a) and 96 h (b) or rotenone for 24 h (c) and 96 h (d) induced a significant  
 166 decrease in  $\beta$ III tubulin level. Data are presented as boxplots, in which each dot represents an independent  
 167 cell population (n=4) in duplicate. Kruskal-Wallis test (one-way ANOVA on ranks) pair-wise (control vs  
 168 6-OHDA or control vs rotenone) was used to assess statistical significance, (\*)  $p < 0.05$ .  
 169 Immunofluorescence images of  $\beta$ III tubulin in differentiated SH-SY5Y cells were acquired using a 20x  
 170 objective and the IN Cell Analyzer 2200. Scale bar = 20  $\mu$ m. Nuclei staining is presented in blue and  $\beta$ III  
 171 tubulin is presented in green (e and f). Cells were treated for 24 h (e) or 96 h (f) with 6.25 (ii), 12.5 (iii), 25  
 172 (iv) and 50  $\mu$ M (v) of 6-OHDA or with 31.25 (vi), 62.5 (vii), 125 (viii) and 250 nM (ix) rotenone. Non-  
 173 treated cells are presented in part (i) of both (e) and (f) panels.

174

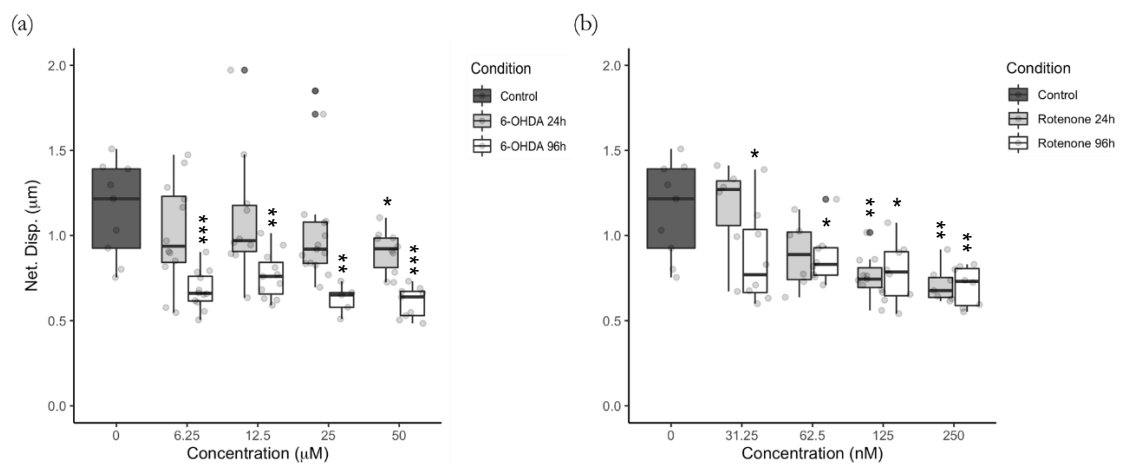
175 **2.3. Mitochondrial net displacement is decreased by treatment with 6-OHDA and**  
 176 **rotenone.**

177

178 Treatment with 50  $\mu$ M 6-OHDA for 24 h resulted in significantly smaller mitochondrial  
 179 net displacement. When incubated for 96 h, all 6-OHDA concentrations substantially

180 decreased mitochondrial net displacement in differentiated SH-SY5Y cells when  
 181 compared to their control counterparts (Fig 3 a). Incubation with 62.5 nM rotenone for  
 182 24 h resulted, on average, in a 22% reduction of mitochondria net displacement, reaching  
 183 statistical significance at 125 and 250 nM. Cells treated for 96 h with rotenone presented  
 184 a significant decrease in mitochondrial net displacement when compared to untreated  
 185 counterparts (Fig 3 b).

186



187

188

189 **Fig 3 – 6-OHDA (a) and rotenone (b) reduced mitochondrial net displacement.**

190 Mitochondria were labeled with the fluorescent dye MitoTracker Red CMXRos, their movement followed,  
 191 and trajectory net displacement was calculated as stated in Materials and Methods. Data are presented as  
 192 boxplots, in which each dot represents the mean of each mitochondrial movement per video frame (n=5 to  
 193 15). Kruskal-Wallis test (one-way ANOVA on ranks) pair-wise (control vs 6-OHDA or control vs rotenone)  
 194 was used to assess statistical significance, (\*\*\*) p < 0.001 (\*\*), p < 0.01, (\*) p < 0.05.

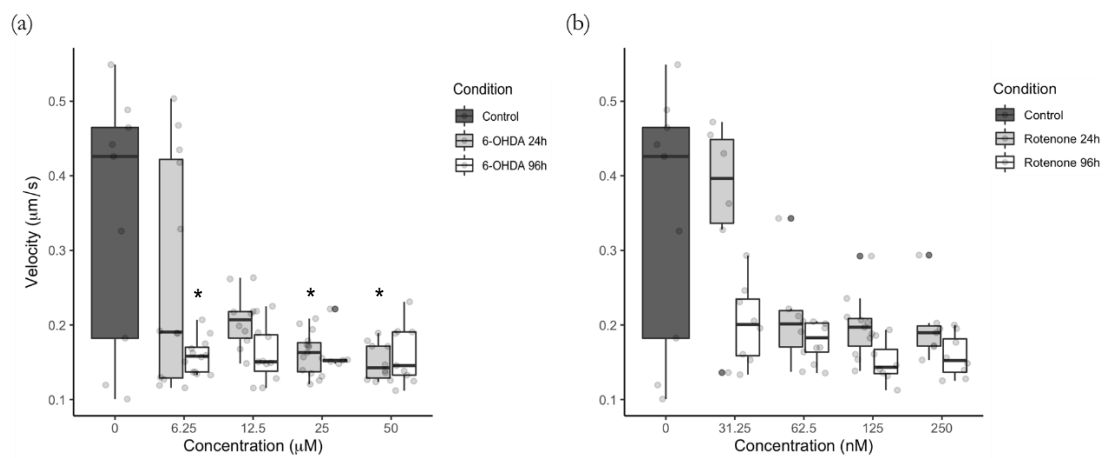
195

196 **2.4. Mitochondrial mean velocity is decreased by treatment with 6-OHDA and**  
 197 **rotenone.**

198

199 Our results indicated that mitochondria move in control cells with the rate of 0.1 to 0.6  
 200 µm/s. (Fig 4 a). Differentiated SH-SY5Y cells treated with 6-OHDA for 24 h exhibited a

201 significant decrease in mitochondria mean velocity when incubated with 25  $\mu\text{M}$  and 50  
 202  $\mu\text{M}$ . Cells incubated with 12.5  $\mu\text{M}$ , 25  $\mu\text{M}$  and 50  $\mu\text{M}$  6-OHDA for 96 h showed  
 203 mitochondrial movement, on average, 55% slower than mitochondria in untreated cells,  
 204 reaching statistical significance when treated with 6.25  $\mu\text{M}$  (Fig 4 a). Rotenone-treated  
 205 cells incubated with 125 nM and 250 nM for 96 h revealed 55% slowed movement of  
 206 mitochondria, although this did not reach significance (Fig 4 b).  
 207



208

209

210 **Fig 4 – Mitochondrial mean velocity is lower due to 6-OHDA (a) and rotenone (b) treatment.**

211 Mitochondria were labeled with the fluorescent dye MitoTracker Red CMXRos, their movement followed,  
 212 and trajectory mean velocity was calculated as stated in Materials and Methods. Data are presented as  
 213 boxplots in which each dot represents the mean of each mitochondrial movement per video frame (n=5 to  
 214 15). Kruskal-Wallis test (One-way ANOVA on ranks) pair-wise (control vs 6-OHDA or control vs  
 215 rotenone) was used to assess statistical significance, (\*)  $p < 0.05$ .

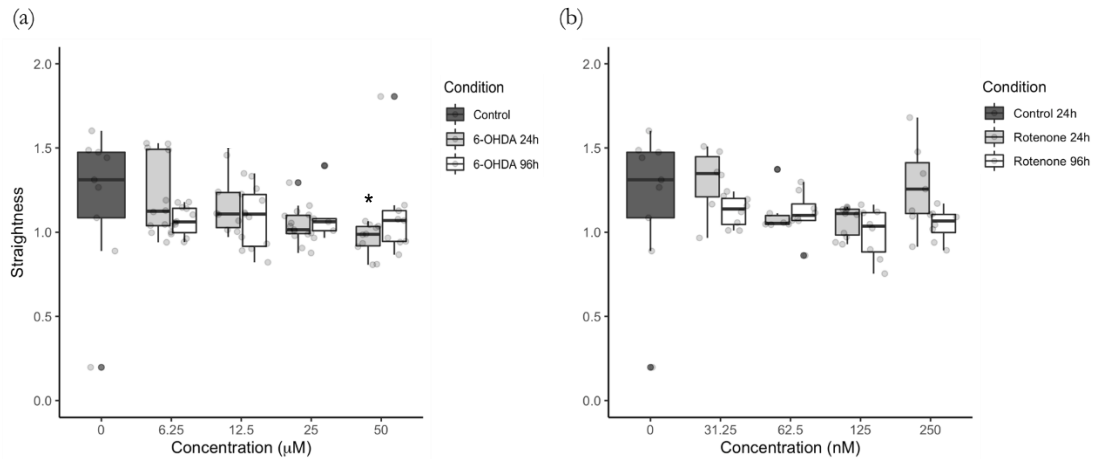
216

217 **2.5. Mitochondrial movement trajectory is affected by 6-OHDA and rotenone.**

218

219 Concerning mitochondria trajectory straightness, mitochondria in cells treated for 24 h  
 220 with 50  $\mu\text{M}$  6-OHDA showed non-straight movement trajectories when compared to  
 221 control cells. The other concentrations of 6-OHDA caused only minor alteration of

222 mitochondrial movement trajectories (Fig 5 a). Rotenone at 125 nM induced a 17%  
223 decrease in mitochondria trajectory straightness although this was not significantly  
224 different from parental cells. No alterations were found for the other rotenone  
225 concentrations (Fig 5 b).



226

227

228 **Fig 5 – Mitochondrial movement pattern straightness was affected in cells treated with 6-OHDA (a)**  
229 **and rotenone (b).**

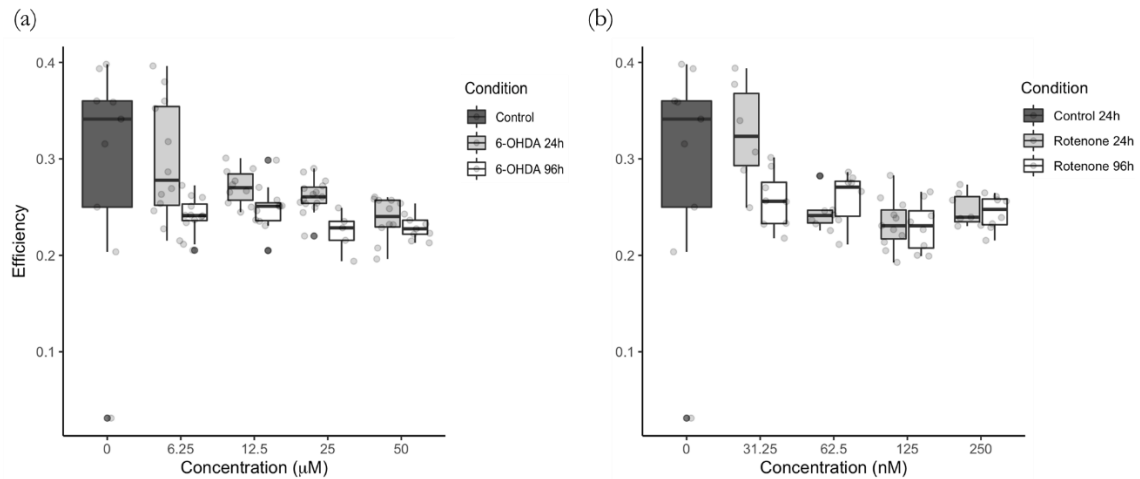
230 Mitochondria were labeled with the fluorescent dye MitoTracker Red CMXRos, their movement followed,  
231 and trajectory straightness was calculated as stated in Materials and Methods. Data are presented as  
232 boxplots in which each dot represents the mean of each mitochondria movement per video frame (n=5 to  
233 15). Kruskal-Wallis test (One-way ANOVA on ranks) pair-wise (control vs 6-OHDA or control vs  
234 rotenone) was used to assess statistical significance, (\*) p< 0.05.

235

236 Regarding individual mitochondria, the trajectory efficiency was small even in control  
237 cells (0.2 to 0.4) (Fig 6 a and b). Cells treated for 96 h with 6.25 µM, 12.5 µM, 25 µM  
238 and 50 µM 6-OHDA showed, on average, a decrease in 17%, 13%, 24% and 21%,  
239 respectively, in mitochondrial trajectory efficiency. Regarding cells treated for 24 h, the  
240 highest 6-OHDA concentration (50 µM) resulted in a 17% average decrease in  
241 mitochondria trajectory efficiency (Fig 6 a). Treatment with 62.5 nM for 24 h and with

242 125 nM rotenone (both 24 h and 96 h) displayed an average 15%, 21% and 21% decrease  
243 of mitochondrial trajectory efficiency when compared to control cells (Fig 6 b).

244



245

246

247 **Fig 6 – Mitochondrial trajectory efficiency was decreased in cells treated with 6-OHDA (a) and with**  
248 **rotenone (b).**

249 Mitochondria were labeled with the fluorescent dye MitoTracker Red CMXRos, their movement followed,  
250 and trajectory efficiency was calculated as stated in Materials and Methods. Data are represented as  
251 boxplots in which each dot represents the mean of each mitochondria movement per video frame (n=5 to  
252 15). Kruskal-Wallis test (One-way ANOVA on ranks) pair-wise (control vs 6-OHDA or control vs  
253 rotenone) was used to assess statistical significance.

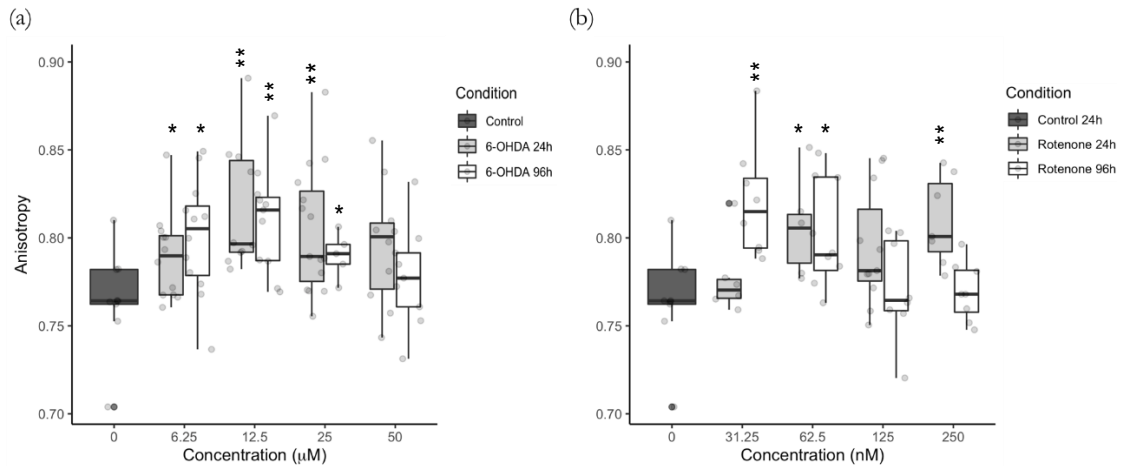
254

255 **2.6. Mitochondria in cells treated with 6-OHDA and rotenone exhibit a higher**  
256 **degree of trajectory anisotropy.**

257

258 Cells incubated for 24 h and 96 h with 6-OHDA at all concentrations, with the exception  
259 of the highest concentration (50  $\mu\text{M}$ ) for both time points, showed a significant increase  
260 in mitochondrial trajectory anisotropy, which was reflected by more unidimensional  
261 trajectories (Fig 7 a). Regarding rotenone, the profile was different in 24 h treated cells.  
262 Mitochondria in cells incubated for 96 h with the lower rotenone concentrations, 31.25

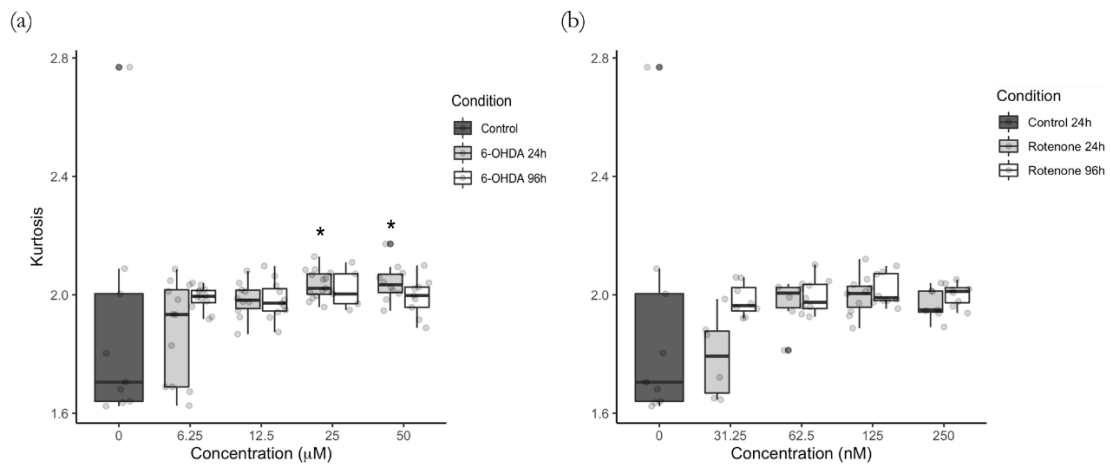
263 nM and 62.5 nM, showed significantly higher degree of trajectory anisotropy, exhibiting  
 264 a more unidimensional trajectory. However, cells treated for 24 h with rotenone at 62.5  
 265 nM and 250 nM of rotenone showed a significant elevation of the degree of mitochondrial  
 266 trajectory anisotropy (Fig 7 b).  
 267



268 **Fig 7 – 6-OHDA (a) and rotenone (b) promote higher degree of mitochondrial movement anisotropy.**  
 269  
 270 Mitochondria were labeled with the fluorescent dye MitoTracker Red CMXRos, their movement followed,  
 271 and trajectory anisotropy was calculated as stated in Materials and Methods. Data are represented as  
 272 boxplots in which each dot represents the mean of each mitochondria movement per video frame (n=5 to  
 273 15). Kruskal-Wallis test (One-way ANOVA on ranks) pair-wise (control vs 6-OHDA or control vs  
 274 rotenone) was used to assess statistical significance, (\*\*), p < 0.01, (\*) p < 0.05.  
 275

276  
 277 **2.7. Shorter incubation times with 6-OHDA enhance kurtosis of mitochondrial**  
 278 **movement pattern.**  
 279

280 Significant increase of mitochondrial trajectory kurtosis was observed in cells treated for  
 281 24 h with the with 6-OHDA at 25 μM and 50 μM (Fig 8 a). On the other hand, no changes  
 282 in kurtosis were observed for cells treated with 6-OHDA at the lower concentrations (Fig  
 283 8 a) and with rotenone at all concentrations (Fig 8 b).  
 284



285

286

287 **Fig 8 – Kurtosis of mitochondrial movement and the effect of 6-OHDA (a) and rotenone (b).**

288 Mitochondria were labeled with the fluorescent dye MitoTracker Red CMXRos, their movement followed,  
 289 and trajectory kurtosis was calculated as stated in Materials and Methods. Data are represented as boxplots  
 290 in which each dot represents the mean of each mitochondria movement per video frame (n=5 to 15).  
 291 Kruskal-Wallis test (One-way ANOVA on ranks) pair-wise (control vs 6-OHDA or control vs rotenone)  
 292 was used to assess statistical significance, (\*) p< 0.05.

293

294 **2.8. Principal component analysis distinguishes control and treated cells.**

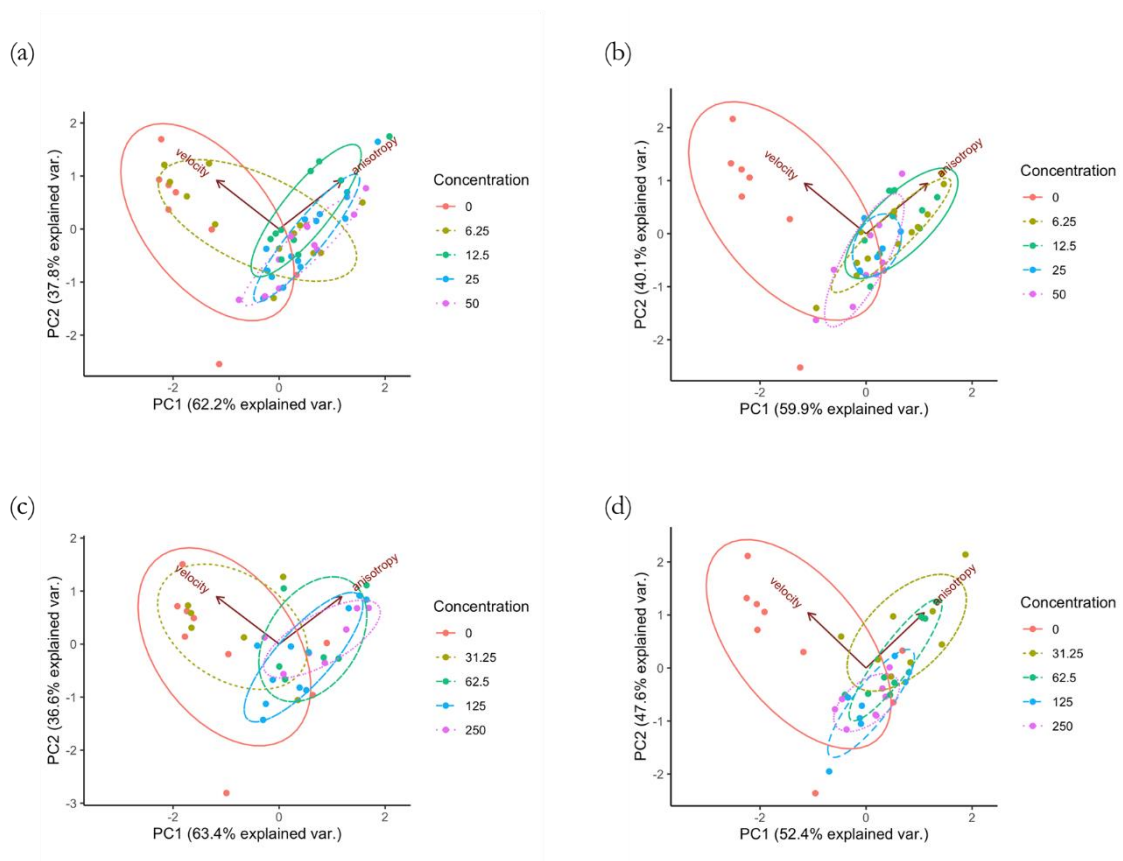
295

296 We performed PCA using the R stats library. The data were zero-centered and scaled to  
 297 obtain unit variance before the analysis (z-score normalization) (31). In Fig 9, we show  
 298 the PCA evaluation with the ellipses centered at the mean vector of the data points, which  
 299 provide a visual intuition of the covariance (32). Treatments with 6-OHDA for 24 h  
 300 presents a significant separation from the control (with variances of 62.2% and 37.8%),  
 301 except for the lowest concentration (6.25 μM), at which the cluster shows a considerable  
 302 superposition with control (Fig 9 a). The same pattern was observed for cells treated with  
 303 rotenone for 24 h (with variances of 63.4% and 36.6%), in which the treatments data  
 304 formed distinct clusters when compared to the control ones. However, the PCA shows  
 305 essentially no difference between the control cells and those treated with 31.25 nM



306 rotenone. For higher concentrations, a clockwise rotation of the principal axes with  
 307 relation to control was observed, with higher variance along the anisotropy direction (Fig  
 308 9 b). In addition, for 96 h treatments with 6-OHDA (with variances 59.9% and 40.1%)  
 309 (Fig 9 c) or rotenone (with variances 52.4% and 47.6%) (Fig 9 d), we observed that the  
 310 results were grouped far from the control, indicating that a longer period of treatment may  
 311 overcome the weak effect associated with lower concentrations. The data ellipses showed  
 312 a trend for a covariance decrease as the concentration of 6-OHDA and rotenone increase  
 313 for the 96 h treatments.

314



315

316 **Fig 9 – The panel shows PCAs for control together with each different treatment: 6-OHDA for 24 h**  
 317 **(a) and 96 h (b) and rotenone for 24 h (c) and 96 h (d).**

318 The normal data ellipses are superposed. Only the two best features that better distinguish between the  
 319 treatments and control conditions were considered, i.e. velocity and anisotropy. In general, the treatments

320 grouped far from the control and presented higher variance along the anisotropy direction, apart from the  
321 treatments for 24 h with lowest concentration of 6-OHDA and rotenone.

322

### 323 **3. Discussion**

324

325 In recent years, the improvement of microscopy methods (enabling the acquisition of high  
326 signal-to-noise images) together with the development of automated particle tracking  
327 algorithms with certain level of accuracy allowed for the analysis of mitochondrial  
328 motility. However, a very careful and critical analysis should be performed when  
329 evaluating mitochondrial trafficking. A prime example is the study of mitochondrial mean  
330 velocity. It has been demonstrated that, depending on the cell model as well as method of  
331 mitochondrial tracking and movement analysis, the values of this parameter could range  
332 from an average of 0.1  $\mu\text{m/s}$  to 1.5  $\mu\text{m/s}$  (20, 21, 23, 33). To the best of our knowledge,  
333 no studies of mitochondrial trafficking have been performed using SH-SY5Y cells. Since  
334 we found that the rate of mitochondrial movement using these cells is 0.1-0.6  $\mu\text{m/s}$ , SH-  
335 SY5Y cells present a plausible model for these studies.

336 In order to provide novel insights into mitochondria trajectory analysis and efficiency, we  
337 treated differentiated SH-SY5Y cells with 6-OHDA or rotenone and performed a more  
338 detailed analysis than carried out in previous studies presented in the literature. A key  
339 enhancement of our approach is the adoption of a wider range of features that help to  
340 characterize mitochondrial trajectories (such as their anisotropy, kurtosis, straightness  
341 and efficiency). A similar approach has been previously applied to the study of human  
342 natural killer cell migration in culture (34) and diffusion of nanoparticles in cellular  
343 microenvironment (35).

344 6-OHDA is a neurotoxic agent known to disrupt mitochondrial trafficking (36, 37). This  
345 substance is a hydroxylated analogue of the neurotransmitter dopamine (38) that induces

346 mitochondrial toxicity by inhibiting complex I function, ensuing in superoxide production  
347 (39). 6-OHDA can also inhibit complex IV (40). Cells treated with 6-OHDA for 96 h  
348 exhibited a more indirect and less efficient trajectory featuring higher anisotropy. This  
349 may be explained by the negative synergistic effect of a significant decrease in ATP level  
350 and the level of  $\beta$ III tubulin. Thus, 6-OHDA alters cell bioenergetics and microtubular  
351 tracks that are both indispensable for mitochondrial movement, ultimately resulting in a  
352 strong effect on dynamics of mitochondrial trafficking. Mitochondria trajectories in cells  
353 treated with this compound for 24 h presented, for higher concentrations (25  $\mu$ M and 50  
354  $\mu$ M), a decrease in straightness, efficiency and net displacement but an increase in  
355 kurtosis. This weaker effect at shorter treatment times is possibly due to a smaller impact  
356 in reducing ATP levels.

357 Changes in mitochondrial trafficking have been described in cells treated with 6-OHDA.  
358 In a study using Lund human mesencephalic cells treated with 6-OHDA at 40  $\mu$ M, 100  
359  $\mu$ M and 250  $\mu$ M for 4 h and 7 h showed a decrease in the number of mitochondria moving  
360 both in the anterograde and retrograde direction without affecting the rate of  
361 mitochondrial movement (37). Similarly, it was shown that treatment with 60  $\mu$ M 6-  
362 OHDA for 30 min in dopaminergic neurons decreased mitochondrial motility by  
363 approximately 50%. Again, no velocity alteration was evident under this scenario (36).  
364 Microtubule modifications and dynamics are also involved in 6-OHDA-related  
365 mitochondrial trafficking impairment. Related to our model, retinoic acid-differentiated  
366 SH-SY5Y cells treated with 30  $\mu$ M 6-OHDA showed tubulin acetylation, which resulted  
367 in decreased microtubule growth rate, and increased level of monomeric tubulin,  
368 suggesting tubulin depolymerization. This effect was attributed to oxidative  
369 modifications of molecules of tubulin (41).

370 Rotenone is a time-dependent high-affinity irreversible inhibitor of complex I (42-44).  
371 This compound leads to inhibition of oxidative phosphorylation and oxygen  
372 consumption, ultimately triggering a cellular bioenergetic deficit. This agent induces  
373 oxidative damage of proteins, lipids and nucleic acids by means of generation of high  
374 levels of superoxide anion (45-47). Rotenone-treated cells showed weaker effect, when  
375 compared to their 6-OHDA-treated counterparts, when assessing the trajectory properties,  
376 which are a focus of this study. Although ATP levels and the level of  $\beta$ III tubulin were  
377 decreased, no evident alterations were found in the trajectory straightness and kurtosis.  
378 Rotenone treatment, despite increasing anisotropy, indicated a more unidimensional  
379 trajectory and decreased trajectory efficiency.

380 Besides being involved in mitochondrial complex I inhibition, affecting ATP and  
381 superoxide anion production, neuronal cells treated with rotenone, both acutely and  
382 chronically, display alterations in mitochondrial trafficking. One study showed that  
383 primary cortical neurons acutely treated with 1  $\mu$ M rotenone exhibited an increase in the  
384 number of stationary mitochondria. Additionally, a significant decrease in the mean  
385 velocity of mitochondrial movement in both directions was also reported (24). Using  
386 differentiated SH-SY5Y cells, it was shown that treatment of the cells with 50 nM  
387 rotenone for 8 and 16 days significantly suppressed the rate of mitochondrial trafficking.  
388 The authors hypothesized that the decrease in mitochondrial velocity was due to either  
389 the disruption of the microtubular network or oxidative stress (48). Indeed, several studies  
390 have shown that rotenone destabilizes microtubules, inducing tubulin depolymerization.  
391 Dopaminergic neurons incubated with 100 nM rotenone for 30 min displayed a significant  
392 increase in free tubulin (49). Additionally, incubation of cells with 10  $\mu$ M rotenone for  
393 12 h induced microtubule depolymerization and blocked its re-polymerization in a similar  
394 cell model (50). using non-neuronal cells, it was shown that rotenone induces tubulin

395 conformational changes, affecting its secondary structure. This suppressed microtubule  
396 re-assembly and decreased the length of microtubules (51).

397 Examining one of the most frequently analyzed features of mitochondrial movement,  
398 which is the mean velocity of mitochondria along tubulin tracks, together with a rarely  
399 assessed feature of mitochondrial mobility, i.e. the anisotropy of mitochondrial  
400 trajectories, we were able to clearly distinguish between cells treated with neuronal  
401 poisons epitomized by 6-OHDA and rotenone. This was particularly evident at the longer  
402 treatment times of 96 h. By considering mean velocity and anisotropy combined with the  
403 PCA projection, we observed that the dispersion in velocity decreases with the treatment  
404 while for anisotropy increases. This behavior was observed in retinoic acid-differentiated  
405 SHSY5Y cells treated with both agents, also presenting a tendency for decreased variance  
406 in anisotropy for longer treatments (96 h) and for higher concentrations of 6-OHDA (50  
407  $\mu\text{M}$ ) and rotenone (250 nM).

408

#### 409 **4. Conclusion**

410

411 This study presents an innovative approach to quantitative analysis of mitochondria  
412 movement in differentiated SH-SY5Y cells treated with neuronal toxins at a range of  
413 concentrations and for different time points. Additionally to the conventionally studied  
414 movement characteristics such as mitochondrial net displacement and mean velocity, we  
415 introduced, for the first time, new movement descriptors to characterize mitochondria  
416 trajectories, i.e. their straightness, efficiency, anisotropy and kurtosis. We have  
417 demonstrated here for the first time that these new descriptors provide an insight into  
418 mitochondrial motility characteristics and can be used to characterize mitochondrial  
419 trajectories. Moreover, in cases in which mitochondrial length of movement and the

420 movement duration, direction and velocity are not altered, these new trajectory  
421 descriptors can present a reliable and sensitive method to detect, in particular, the initial  
422 stages of neuronal degeneration.

423

## 424 **5. Material and methods**

425

### 426 **5.1. Cell culture and treatments**

427

428 SH-SY5Y cells (ECACC, cat. 94030304) were cultured in supplemented Dulbecco's  
429 modified Eagle's medium (DMEM, D5030, Sigma-Aldrich, USA) and differentiated into  
430 a neuronal-like morphology following a protocol published by us (52). Details are  
431 provided in the S1 Appendix.

432

### 433 **5.2. ATP levels determination**

434

435 Intracellular ATP was quantified using the CellTiter-Glo Luminescent Cell Viability  
436 Assay (G7570, Promega, USA) following manufacture's protocol. Details are provided  
437 in the S1 Appendix.

438

### 439 **5.3. Immunocytochemistry and fluorescence microscopy**

440

441  $\beta$ III tubulin (sc80005, Santa Cruz, Germany) levels and Hoechst 33342 (B2261, Sigma-  
442 Aldrich) nuclear labelling in fixed SH-SY5Y cells were assessed following the protocol  
443 described in the S1 Appendix.

444

445

446

447 **5.4. Live cell imaging**

448

449 For live imaging, cells were differentiated in 35 mm  $\mu$ -dishes (81156, Ibidi Germany) at  
450  $3 \times 10^4$  cells/cm<sup>2</sup> and treated with 6-OHDA and rotenone. Subsequently, mitochondria  
451 were stained with 25 nM of the mitochondrial fluorescent dye MitoTracker Red CMXRos  
452 (M7512, Invitrogen, Thermo Fisher Scientific) in the FluoroBrite DMEM Media  
453 (A1896702, Gibco, Thermo Fisher Scientific) for 30 min. The media was then replaced  
454 by fresh FluoroBrite DMEM Media. Movies of fluorescent mitochondria were then  
455 recorded using the TIRF-fitted Nikon Eclipse Ti2 inverted microscope. The lowest level  
456 of excitation light from the 561 nm laser was used for imaging, and the emitted light was  
457 collected using an mCherry filter. The EMCCD Andor iXon Ultra DU888 camera (Andor  
458 Technologies) was used to capture the images with resolution of 1024 x 1024 pixels (pixel  
459 size 13 x 13  $\mu$ m) at 1 frame per second for 10 min.

460

461 **Movie Processing**

462

463 Raw movie files were convolved and filtered using ImageJ. After applying noise  
464 reduction, they were saved as a sequence of binary images. A MATLAB algorithm  
465 ([www.github.com/kandelj/MitoSPT](http://www.github.com/kandelj/MitoSPT)) (53) was then used to detect object movement  
466 across frames, allowing for the calculation of the trajectory, total and net distances  
467 traveled by each individual mitochondria. Movie processing details are provided in the  
468 S1 Appendix.

469

470

471

## 472 **5.5. Quantitative analysis of trajectories**

473

474 Specific physical properties, describing the curve shape and kinematics of individual  
475 mitochondria trajectories, were obtained with the python package trajpy (54, 55),  
476 available at <https://github.com/ocbe-uo/trajpy/>. Supplementary figures in S2 Appendix  
477 display some examples of trajectories. The calculated trajectory features are the  
478 following.

479

### 480 5.5.1. Mean velocity

481

482 We evaluated the mitochondria mean velocity  $\langle v \rangle$  by calculating the ratio between the  
483 total length of the trajectory and the elapsed time  $\Delta t$

$$484 \quad \langle v \rangle = \frac{\sum_{i=1}^{N-1} |\mathbf{r}_{i+1} - \mathbf{r}_i|}{\Delta t}, \quad (1)$$

485 where  $N$  is the number of segments of the trajectory, and  $\mathbf{r}_i$  is the position of the  $i$ -th point  
486 along the trajectory path.

487

### 488 5.5.2. Anisotropy

489

490 The features related to the trajectory shape are functions of the gyration tensor obtained  
491 by the variance of the position along the trajectory. Mathematically, the components of  
492 the gyration tensor,  $R_{mn}$ , are given by the following equation:

$$493 \quad R_{mn} = \frac{1}{2N^2} \sum_{i=1}^N \sum_{j=1}^N (r_{m,i} - r_{m,j}) (r_{n,i} - r_{n,j}), \quad (2)$$

494 in which  $m$  and  $n$  are indices for the coordinates along the directions  $x$ ,  $y$ ,  $z$ .

495 Using the diagonalized gyration tensor  $D$  to define the tensor,  $\hat{R} = D - 1/3(TrD)\mathbb{1}$  with  
496 the unity tensor  $\mathbb{1}$ , we obtained the degree of anisotropy among the principal axes (56),  
497 defined as



498 
$$k^2 \equiv \frac{3}{2} \frac{Tr\hat{R}^2}{(Tr\hat{R})^2}, \quad (3)$$

499

500 where, the setting  $Tr\hat{R} = \lambda_1 + \lambda_2 + \lambda_3$ , gives

501 
$$k^2 = 1 - 3 \frac{\lambda_1\lambda_2 + \lambda_2\lambda_3 + \lambda_3\lambda_1}{(\lambda_1 + \lambda_2 + \lambda_3)}. \quad (4)$$

502 The minimum anisotropy,  $k^2 = 0$ , is obtained when the distribution of the trajectory  
 503 points is spherically symmetrical with  $\lambda_1 = \lambda_2 = \lambda_3$ . The maximum anisotropy,  $k^2 = 1$ ,  
 504 occurs when at least two eigenvalues are zero. High anisotropy refers to a small  
 505 dimensionality in the principal axes coordinates - unidimensional trajectories present the  
 506 highest anisotropy. Thus, anisotropy carries information about symmetry and  
 507 dimensionality at the same time (57).

508

### 509 5.5.3. Kurtosis

510

511 We obtained the kurtosis of the trajectory by projecting each position along the main  
 512 principal eigenvector of the radius of the gyration tensor  $r_i^p = \mathbf{r}_i \cdot \mathbf{e}_{\lambda_1}$ , in which  $\mathbf{e}_{\lambda_1}$  is  
 513 the eigenvector associated to the eigenvalue  $\lambda_1$ , and then calculating the quartic moment

514 
$$K = \frac{1}{N} \sum_{i=1}^N \frac{(r_i^p - \langle r^p \rangle)^4}{\sigma_{r^p}^4}, \quad (5)$$

515 in which  $\langle r^p \rangle$  is the mean position of the projected trajectory and  $\sigma_{r^p}^2$  is its variance.

516 Kurtosis is the measure of the ‘tailedness’ of the positions distribution in the trajectory  
 517 (58).

518

### 519 5.5.4. Straightness

520

521 Straightness compares the net displacement to the sum of displacements. It measures the  
 522 likeliness of the trajectory to a straight line

523 
$$S = \frac{|\mathbf{r}_N - \mathbf{r}_1|}{\sum_{i=1}^{N-1} |\mathbf{r}_{i+1} - \mathbf{r}_i|}, \quad (6)$$

524 where  $\mathbf{r}_1$  is the initial position and  $\mathbf{r}_N$  is the last position on the trajectory. If the trajectory  
525 is completely straight, the numerator and denominator are the same, consequently  $S = 1$ .  
526 On the other hand, if  $\sum_{i=1}^{N-1} |\mathbf{r}_{i+1} - \mathbf{r}_i| \gg \mathbf{r}_N - \mathbf{r}_1$ , then  $S \approx 0$ .

527

### 528 5.5.5. Efficiency

529

530 Efficiency is similar to straightness described above. It is defined as the ratio between the  
531 net displacement and the sum of squared displacements:

$$532 \quad E_{ff} = \frac{|\mathbf{r}_N - \mathbf{r}_1|^2}{\sum_{i=1}^{N-1} |\mathbf{r}_{i+1} - \mathbf{r}_i|^2} \quad (7)$$

533 When a particle describes a long trajectory but ends at the same initial position, the  
534 measured efficiency will be zero. Moreover, for the same net displacement, a highly  
535 irregular trajectory will have smaller efficiency than the linear trajectory.

536

## 537 **5.6. Statistics**

538

539 Data were analyzed using R 4.0.3 (31). Results are presented in boxplots (box-and-  
540 whisker plots), in which the middle line represents the median and the whiskers go down  
541 to the minimum value and up to the maximum value, where each individual value is  
542 represented as a data point. The number of experiments carried out is presented in the  
543 legend of the figures.

544 We performed the non-parametric Kruskal-Wallis test pair-wise comparisons between the  
545 control and each treatment condition followed by Dunn's post hoc for multiple conditions  
546 comparison. Statistical significance was set as (\*)  $p < 0.05$ , (\*\*)  $p < 0.01$ , (\*\*\*)  $p < 0.001$   
547 and (\*\*\*\*)  $p < 0.0001$ . Principal component analysis (PCA) was employed to identify the  
548 underlying covariable patterns of the data.

549

550

551 **Funding**

552

553 This work was funded by Montepio Foundation and FEDER/COMPETE/national funds  
554 by FCT under research grants PTDC/BTM-SAL/29297/2017, POCI-01-0145-FEDER-  
555 029297 (MitoScreening), UIDB/04539/2020 (CNC Strategic Plan), PTDC/MED-  
556 FAR/29391/2017, POCI-01-0145-FEDER-029391 (Mito4ALS), UIDB/04564/2020.  
557 R.F. Simões (PD/BD/128254/2016) was supported by ERDF through COMPETE  
558 2020/FCT. JN was supported in part by the grant 21-04607X from the Czech Science  
559 Foundation. M. M-S was supported by European Union's Horizon 2020 research and  
560 innovation programme under the Marie Skłodowska-Curie grant agreement No 801133.

561

562 **S1 Appendix**

563

564 **Cell culture and differentiation**

565

566 SH-SY5Y cells (ECACC, cat. 94030304) were cultured in Dulbecco's modified Eagle's  
567 medium (DMEM, D5030, Sigma-Aldrich, USA) containing 25 mM glucose (G7021,  
568 Sigma-Aldrich), 6 mM L-glutamine (G3126, Sigma-Aldrich), 5 mM HEPES (H4024,  
569 Sigma-Aldrich), 44 mM sodium bicarbonate (S6014, Sigma-Aldrich), 1 mM sodium  
570 pyruvate (P2256, Sigma-Aldrich), 10% (v/v) fetal bovine serum (41F6445K, Gibco,  
571 Thermo Fisher Scientific, USA) and 1% penicillin/streptomycin (1772652 Thermo Fisher  
572 Scientific) in a humidified atmosphere (5% CO<sub>2</sub>, 37 °C). Cell media was changed every  
573 2 to 3 days, and cells were split when reaching 90-100% confluency.

574 For cell differentiation, cells were seeded at the density of  $3 \times 10^4$  cells/cm<sup>2</sup> in low glucose  
575 (5 mM) media supplemented with 1% FBS and 10  $\mu$ M retinoic acid (RA) (A6947 Panreac  
576 AppliChem ITW Reagents, Germany) for 3 days. Following differentiation, cells were  
577 treated with increasing concentration of 6-OHDA (H4381 Sigma-Aldrich) or rotenone  
578 (MKBS1062V, Sigma-Aldrich).

579

#### 580 **ATP levels determination**

581

582 Cell differentiation and treatments were accomplished in white, opaque-bottom, 96-well  
583 plates (136101, Thermo Fisher Scientific). At the end of cell treatments, the medium was  
584 removed and replaced by 50  $\mu$ l of fresh medium. 50  $\mu$ l of the Cell Titer-Glo reagent was  
585 added, and plates were agitated for 2 min on an orbital shaker to promote cell lysis. After  
586 10-min incubation, the luminescent signal was recorded using Cytation™ 3 microplate  
587 reader (BioTek, USA).

588

#### 589 **Immunocytochemistry and fluorescence microscopy**

590

591 After cell differentiation and treatment, the cell culture medium was removed, cells were  
592 washed with warm phosphate buffer saline (PBS), fixed with 4% paraformaldehyde in  
593 PBS and stored at 4 °C. The cells were then washed 3 times with PBS and permeabilized  
594 with 0.2% (v/v) Triton X-100 (AC327371000, Fisher Scientific) in PBS for 2 min. The  
595 cells were then washed 3 times with PBS, and incubated with the blocking solution (3%  
596 bovine serum albumin, BSA; A6003 Sigma-Aldrich) in PBS. The cells were washed 3  
597 times with PBS containing 1% BSA and incubated overnight at 4 °C with mouse anti- $\beta$ III  
598 tubulin (sc80005, Santa Cruz, Germany) at 1:200 dilution prepared in 3% BSA in PBS.

599 This was followed by 90-min incubation with goat-anti-mouse Alexa Fluor 488 (A-  
600 11001, Cat. M7512, Invitrogen, Thermo Fisher Scientific, USA) at 1:1000 dilution in 3%  
601 BSA in PBS. Finally, cells were washed 3 times with 1% BSA in PBS and incubated with  
602 1 µg/ml Hoechst 33342 (B2261, Sigma-Aldrich) in PBS for nuclei visualization.  
603 Cell visualization was performed using an INCell Analyzer 2200 (GE Healthcare) cell  
604 imaging system. Images were acquired using a 20x objective (INCA ASAC 20 x/0.45,  
605 ELWD Plan Fluor). Image analysis was performed using the INCell Analyzer 1000  
606 analysis software - Developer Toolbox. The image stack was uploaded by the software to  
607 identify our target set and to establish the respective parameters of area and number. The  
608 representative images shown in this work were visualized using ImageJ 1.52a (Wayne  
609 Rasband, National Instituted of Health, USA).

610

### 611 **ImageJ image pre-processing**

612

613 Following the published protocol (53), we pre-processed raw image files using ImageJ.  
614 Briefly, time-lapse images were first convolved using the 5×5 edge-detection, converted  
615 to the frequency domain using a Fast Fourier Transform, and then subjected to a bandpass  
616 filter ranging from 2 pixels (~0.3 µm) to 100 pixels (~16 µm). The resulting images were  
617 manually thresholded to eliminate the noise, and the results saved as a sequence of  
618 individual binary images.

619

### 620 **MATLAB Algorithm**

621

622 The stacks of individual images were analyzed by an open source MATLAB algorithm  
623 ([www.github.com/kandelj/MitoSPT](http://www.github.com/kandelj/MitoSPT)) (53). Briefly, the algorithm read each frame into

624 MATLAB and used the built-in functions *bwconncomp* and *regionprops* to find the  
625 connected white objects and to measure their sizes, respectively. The image was then  
626 recreated to contain only objects with the area within the specified limits defined by the  
627 user. Each frame went through the same process. The current frame objects were labeled  
628 or re-labeled by comparing their pixel locations with the ones from the previous frame.  
629 After all objects were labeled/re-labeled, their locations were stored, and they were  
630 prepared to be compared with the next frame. After this process was repeated frame by  
631 frame, the collected centroid locations were used to calculate the total and net distances  
632 traveled by each object (53). In addition, the software was adapted to output the raw  
633 trajectories of each individual mitochondria into a comma-separated values file (csv) for  
634 external analysis.

635

## 636 **S2 Appendix - Supplementary figures captions**

637

638 **Supplementary Fig. 1** - A subset of 3 trajectories obtained from the control group.

639

640 **Supplementary Fig. 2** - Three trajectories with different stochastic noise strength  $\gamma = \{0, 6, 20\}$ . This  
641 example is a linear trajectory  $y(x) = x + \gamma(\text{Rand} - 0.5)$  under the influence of a random noise with  
642  $\{x \in \mathbb{R} | 0 \leq x \leq 100\}$  and  $\gamma$  is the parameter that controls the stochastic strength. It is shown the  
643 trajectories for  $\gamma = 0$  (without noise),  $\gamma = 6$  (weak noise) and  $\gamma = 20$  (high noise), presenting lower to  
644 higher tortuosity, respectively.

645

646 **Supplementary Fig. 3** - Circular trajectory to observe the effect of symmetry in the features by considering  
647 subsets of the circle, as exemplified with 6, 11 and 20 points. We calculated the anisotropy, kurtosis,  
648 straightness and efficiency attributes for incomplete circles from 3 to 20 points (complete circle),  
649 counterclockwise, and determined the dependency as a function of the number of points considered.

650

651 **Supplementary Fig. 4** - The effect of stochasticity on each of the features is depicted. We can observe that  
652 anisotropy and kurtosis are resilient to the introduction of stochastic noise in the trajectory. The anisotropy  
653 shows a tendency to decrease as the noise influence increases, while the kurtosis goes in the opposite  
654 direction and increases with  $\gamma$ . In contrast, efficiency and straightness are strongly affected by stochasticity,  
655 decreasing rapidly.

656

657 **Supplementary Fig. 5** - Anisotropy, kurtosis, efficiency and straightness measured for the circular  
658 trajectory with different subsets. We can see that the anisotropy and the kurtosis present a non-monotonic  
659 behavior. As we consider more points in the circle, the anisotropy decreases due to the symmetry of the  
660 circle. With 11 points we have the semi-circle, which coincides with a local minimum in anisotropy and a  
661 local maximum in kurtosis. Efficiency and straightness decrease monotonically as we vary the number of  
662 points. The examples explored here highlight the difficulties faced in the analysis of some features,  
663 presenting often a non-intuitive behavior.

664

665

666

667

668

669

670

671

672

673

674

675

676

677

678

679

680 **References**

681

- 682 1. Sheng ZH, Cai Q. Mitochondrial transport in neurons: impact on synaptic homeostasis  
683 and neurodegeneration. *Nat Rev Neurosci.* 2012;13(2):77-93.
- 684 2. Saxton WM, Hollenbeck PJ. The axonal transport of mitochondria. *J Cell Sci.*  
685 2012;125(Pt 9):2095-104.
- 686 3. Sheng ZH. Mitochondrial trafficking and anchoring in neurons: New insight and  
687 implications. *J Cell Biol.* 2014;204(7):1087-98.
- 688 4. Attwell D, Laughlin SB. An energy budget for signaling in the grey matter of the brain.  
689 *J Cereb Blood Flow Metab.* 2001;21(10):1133-45.
- 690 5. Harris JJ, Jolivet R, Attwell D. Synaptic energy use and supply. *Neuron.*  
691 2012;75(5):762-77.
- 692 6. Sun T, Qiao H, Pan PY, Chen Y, Sheng ZH. Motile axonal mitochondria contribute to  
693 the variability of presynaptic strength. *Cell Rep.* 2013;4(3):413-9.
- 694 7. Billups B, Forsythe ID. Presynaptic mitochondrial calcium sequestration influences  
695 transmission at mammalian central synapses. *J Neurosci.* 2002;22(14):5840-7.
- 696 8. Medler K, Gleason EL. Mitochondrial Ca(2+) buffering regulates synaptic transmission  
697 between retinal amacrine cells. *J Neurophysiol.* 2002;87(3):1426-39.
- 698 9. Schwarz TL. Mitochondrial trafficking in neurons. *Cold Spring Harb Perspect Biol.*  
699 2013;5(6).
- 700 10. Morris RL, Hollenbeck PJ. The regulation of bidirectional mitochondrial transport is  
701 coordinated with axonal outgrowth. *J Cell Sci.* 1993;104 ( Pt 3):917-27.
- 702 11. Pilling AD, Horiuchi D, Lively CM, Saxton WM. Kinesin-1 and Dynein are the primary  
703 motors for fast transport of mitochondria in *Drosophila* motor axons. *Mol Biol Cell.*  
704 2006;17(4):2057-68.
- 705 12. Hirokawa N, Niwa S, Tanaka Y. Molecular motors in neurons: transport mechanisms  
706 and roles in brain function, development, and disease. *Neuron.* 2010;68(4):610-38.
- 707 13. Kapitein LC, Hoogenraad CC. Building the Neuronal Microtubule Cytoskeleton.  
708 *Neuron.* 2015;87(3):492-506.
- 709 14. Nguyen MM, Stone MC, Rolls MM. Microtubules are organized independently of the  
710 centrosome in *Drosophila* neurons. *Neural Dev.* 2011;6:38.
- 711 15. Yau KW, Schatzle P, Tortosa E, Pages S, Holtmaat A, Kapitein LC, et al. Dendrites In  
712 Vitro and In Vivo Contain Microtubules of Opposite Polarity and Axon Formation Correlates  
713 with Uniform Plus-End-Out Microtubule Orientation. *J Neurosci.* 2016;36(4):1071-85.
- 714 16. MacAskill AF, Brickley K, Stephenson FA, Kittler JT. GTPase dependent recruitment  
715 of Grif-1 by Miro1 regulates mitochondrial trafficking in hippocampal neurons. *Mol Cell*  
716 *Neurosci.* 2009;40(3):301-12.
- 717 17. Brickley K, Stephenson FA. Trafficking kinesin protein (TRAK)-mediated transport of  
718 mitochondria in axons of hippocampal neurons. *J Biol Chem.* 2011;286(20):18079-92.
- 719 18. King SJ, Schroer TA. Dynactin increases the processivity of the cytoplasmic dynein  
720 motor. *Nat Cell Biol.* 2000;2(1):20-4.
- 721 19. Ligon LA, Steward O. Movement of mitochondria in the axons and dendrites of  
722 cultured hippocampal neurons. *J Comp Neurol.* 2000;427(3):340-50.
- 723 20. Misgeld T, Kerschensteiner M, Bareyre FM, Burgess RW, Lichtman JW. Imaging  
724 axonal transport of mitochondria in vivo. *Nat Methods.* 2007;4(7):559-61.
- 725 21. Fang C, Bourdette D, Banker G. Oxidative stress inhibits axonal transport: implications  
726 for neurodegenerative diseases. *Mol Neurodegener.* 2012;7:29.
- 727 22. Bros H, Millward JM, Paul F, Niesner R, Infante-Duarte C. Oxidative damage to  
728 mitochondria at the nodes of Ranvier precedes axon degeneration in ex vivo transected axons.  
729 *Exp Neurol.* 2014;261:127-35.
- 730 23. Bros H, Hauser A, Paul F, Niesner R, Infante-Duarte C. Assessing Mitochondrial  
731 Movement Within Neurons: Manual Versus Automated Tracking Methods. *Traffic.*  
732 2015;16(8):906-17.



733 24. Chen M, Li Y, Yang M, Chen X, Chen Y, Yang F, et al. A new method for quantifying  
734 mitochondrial axonal transport. *Protein Cell*. 2016;7(11):804-19.

735 25. Coutu DL, Schroeder T. Probing cellular processes by long-term live imaging--historic  
736 problems and current solutions. *J Cell Sci*. 2013;126(Pt 17):3805-15.

737 26. Gerencser AA, Nicholls DG. Measurement of instantaneous velocity vectors of  
738 organelle transport: mitochondrial transport and bioenergetics in hippocampal neurons. *Biophys*  
739 *J*. 2008;95(6):3079-99.

740 27. Chang DT, Rintoul GL, Pandipati S, Reynolds IJ. Mutant huntingtin aggregates impair  
741 mitochondrial movement and trafficking in cortical neurons. *Neurobiol Dis*. 2006;22(2):388-  
742 400.

743 28. Axelrod D. Chapter 7: Total internal reflection fluorescence microscopy. *Methods Cell*  
744 *Biol*. 2008;89:169-221.

745 29. Mattheyses AL, Simon SM, Rappoport JZ. Imaging with total internal reflection  
746 fluorescence microscopy for the cell biologist. *J Cell Sci*. 2010;123(Pt 21):3621-8.

747 30. Poulter NS, Pitkeathly WT, Smith PJ, Rappoport JZ. The physical basis of total internal  
748 reflection fluorescence (TIRF) microscopy and its cellular applications. *Methods Mol Biol*.  
749 2015;1251:1-23.

750 31. R Core Team. R: A language and environment for statistical computing. R Foundation  
751 for Statistical Computing. Vienna, Austria. 2020 [Available from: [http://www.r-](http://www.r-project.org/index.html)  
752 [project.org/index.html](http://www.r-project.org/index.html)].

753 32. Friendly M, Monette G, Fox J. Elliptical Insights: Understanding Statistical Methods  
754 through Elliptical Geometry. *Statist Sci*. 2013;28(1):1-39.

755 33. MacAskill AF, Kittler JT. Control of mitochondrial transport and localization in  
756 neurons. *Trends Cell Biol*. 2010;20(2):102-12.

757 34. Lee BJ, Mace EM. Acquisition of cell migration defines NK cell differentiation from  
758 hematopoietic stem cell precursors. *Mol Biol Cell*. 2017;28(25):3573-81.

759 35. Wagner T, Kroll A, Haramagatti CR, Lipinski HG, Wiemann M. Classification and  
760 Segmentation of Nanoparticle Diffusion Trajectories in Cellular Micro Environments. *PLoS*  
761 *One*. 2017;12(1):e0170165.

762 36. Lu X, Kim-Han JS, Harmon S, Sakiyama-Elbert SE, O'Malley KL. The Parkinsonian  
763 mimetic, 6-OHDA, impairs axonal transport in dopaminergic axons. *Mol Neurodegener*.  
764 2014;9:17.

765 37. Stepkowski TM, Meczynska-Wielgosz S, Kruszewski M. mitoLUHMES: An  
766 Engineered Neuronal Cell Line for the Analysis of the Motility of Mitochondria. *Cell Mol*  
767 *Neurobiol*. 2017;37(6):1055-66.

768 38. Blum D, Torch S, Lambeng N, Nissou M, Benabid AL, Sadoul R, et al. Molecular  
769 pathways involved in the neurotoxicity of 6-OHDA, dopamine and MPTP: contribution to the  
770 apoptotic theory in Parkinson's disease. *Prog Neurobiol*. 2001;65(2):135-72.

771 39. Betarbet R, Sherer TB, Greenamyre JT. Animal models of Parkinson's disease.  
772 *Bioessays*. 2002;24(4):308-18.

773 40. Glinka YY, Youdim MBH. Inhibition of mitochondrial complexes I and IV by 6-  
774 hydroxydopamine. *European Journal of Pharmacology: Environmental Toxicology and*  
775 *Pharmacology*. 1995;292(3):329-32.

776 41. Patel VP, DeFranco DB, Chu CT. Altered transcription factor trafficking in oxidatively-  
777 stressed neuronal cells. *Biochim Biophys Acta*. 2012;1822(11):1773-82.

778 42. Schuler F, Casida JE. Functional coupling of PSST and ND1 subunits in  
779 NADH:ubiquinone oxidoreductase established by photoaffinity labeling. *Biochim Biophys*  
780 *Acta*. 2001;1506(1):79-87.

781 43. Degli Esposti M. Inhibitors of NADH-ubiquinone reductase: an overview. *Biochim*  
782 *Biophys Acta*. 1998;1364(2):222-35.

783 44. Lummen P. Complex I inhibitors as insecticides and acaricides. *Biochim Biophys Acta*.  
784 1998;1364(2):287-96.

785 45. Sanders LH, Timothy Greenamyre J. Oxidative damage to macromolecules in human  
786 Parkinson disease and the rotenone model. *Free Radic Biol Med*. 2013;62:111-20.

787 46. Sherer TB, Betarbet R, Testa CM, Seo BB, Richardson JR, Kim JH, et al. Mechanism  
788 of toxicity in rotenone models of Parkinson's disease. *J Neurosci*. 2003;23(34):10756-64.  
789 47. Uversky VN. Neurotoxicant-induced animal models of Parkinson's disease:  
790 understanding the role of rotenone, maneb and paraquat in neurodegeneration. *Cell Tissue Res*.  
791 2004;318(1):225-41.  
792 48. Borland MK, Trimmer PA, Rubinstein JD, Keeney PM, Mohanakumar K, Liu L, et al.  
793 Chronic, low-dose rotenone reproduces Lewy neurites found in early stages of Parkinson's  
794 disease, reduces mitochondrial movement and slowly kills differentiated SH-SY5Y neural cells.  
795 *Mol Neurodegener*. 2008;3:21.  
796 49. Jiang Q, Yan Z, Feng J. Neurotrophic factors stabilize microtubules and protect against  
797 rotenone toxicity on dopaminergic neurons. *J Biol Chem*. 2006;281(39):29391-400.  
798 50. Ren Y, Liu W, Jiang H, Jiang Q, Feng J. Selective vulnerability of dopaminergic  
799 neurons to microtubule depolymerization. *J Biol Chem*. 2005;280(40):34105-12.  
800 51. Srivastava AS, Feng Z, Mishra R, Malhotra R, Kim HS, Carrier E. Embryonic stem  
801 cells ameliorate piroxicam-induced colitis in IL10<sup>-/-</sup> KO mice. *Biochem Biophys Res Commun*.  
802 2007;361(4):953-9.  
803 52. Simoes RF, Ferrao R, Silva MR, Pinho SLC, Ferreira L, Oliveira PJ, et al. Refinement  
804 of a differentiation protocol using neuroblastoma SH-SY5Y cells for use in neurotoxicology  
805 research. *Food Chem Toxicol*. 2021;149:111967.  
806 53. Kandel J, Chou P, Eckmann DM. Automated detection of whole-cell mitochondrial  
807 motility and its dependence on cytoarchitectural integrity. *Biotechnol Bioeng*.  
808 2015;112(7):1395-405.  
809 54. Moreira-Soares M. trajpy. 1.3.1 ed: Zenode; 2020.  
810 55. Moreira-Soares M, Cunha SP, Bordin JR, Travasso RDM. Adhesion modulates cell  
811 morphology and migration within dense fibrous networks. *Journal of Physics: Condensed*  
812 *Matter*. 2020;32(31):314001.  
813 56. Theodorou DN, Suter UW. Shape of unperturbed linear polymers: polypropylene.  
814 *Macromolecules*. 1985;18(6):1206-14.  
815 57. Arkin H, Janke W. Gyration tensor based analysis of the shapes of polymer chains in an  
816 attractive spherical cage. *J Chem Phys*. 2013;138(5):054904.  
817 58. Helmuth JA, Burckhardt CJ, Koumoutsakos P, Greber UF, Sbalzarini IF. A novel  
818 supervised trajectory segmentation algorithm identifies distinct types of human adenovirus  
819 motion in host cells. *J Struct Biol*. 2007;159(3):347-58.  
820